Fission cross sections of lead projectiles in Pb-nucleus interactions at 40 and 158 GeV/*c* per nucleon

B. Alessandro,[1] C. Alexa,[2] R. Arnaldi,[1] M. Atayan,[3] C. Baglin,[4] A. Baldit,[5] M. Bedjidian,[6] S. Beolè,[1] V. Boldea,[2] P. Bordalo,[7,*] G. Borges,[7] A. Bussière,[4] L. Capelli,[6] C. Castanier,[5] J. Castor,[5] B. Chaurand,[8] B. Cheynis,[6] E. Chiavassa,[1] C. Cicalò,[9] M. P. Comets,[10] S. Constantinescu,[2] P. Cortese,[11] G. Dellacasa,[11] A. Devaux,[5] A. De Falco,[9] N. De Marco,[1] S. Dita,[2] B. Espagnon,[5] J. Fargeix,[5] A. Ferretti,[1] P. Force,[5] M. Gallio,[1] C. Gerschel,[10] P. Giubellino,[1] M. B. Golubeva,[12] A. A Grigoryan,[3] S. Grigoryan,[3] F. F. Guber,[12] A. Guichard,[6] H. Gulkanyan,[3] M. Idzik,[1,†] D. Jouan,[10] T. L. Karavicheva,[12] L. Kluberg,[8] A. B. Kurepin,[12] Y. Le Bornec,[10] P. Macciotta,[9] M. Mac Cormick,[10] A. Marzari-Chiesa,[1] M. Masera,[1] A. Masoni,[9] M. Monteno,[1] A. Musso,[1] C. Oppedisano,[1] A. Piccotti,[1] J. R. Pizzi,[6] F. Prino,[11] G. Puddu,[9] C. Quintans,[7] L. Ramello,[11] S. Ramos,[7,*] P. Rato Mendes,[7] L. Riccati,[1] H. Santos,[7] P. Saturnini,[5] E. Scalas,[11] E. Scomparin,[1] S. Serci,[9] R. Shahoian,[7,‡] F. Sigaudo,[1] M. Sitta,[11] P. Sonderegger,[13,*] X. Tarrago,[10] N. S. Topilskaya,[12] G. L. Usai,[9] E. Vercellin,[1] L. Villatte,[10] and N. Willis[10]

(NA50 Collaboration)

[1]*Dipartimento di Fisica Sperimentale, Università di Torino and INFN-Torino, Torino, Italy*

[2]*IFA, Bucharest, Romania*

[3]*YerPhI, Yerevan, Armenia*

[4]*LAPP, CNRS-IN2P3, Annecy-le-Vieux, France*

[5]*LPC, Université, Blaise Pascal and CNRS-IN2P3, Aubiére, France*

[6]*Institut de Physique Nucleaire de Lyon (IPNL), Université, Claude Bernard, IN2P3-CNRS, Villeurbanne, France*

[7]*LIP, Lisbon, Portugal*

[8]*Laboratoire Leprince-Ringuet, Ecole Polytechnique and CNRS-IN2P3, Palaiseau, France*

[9]*Università di Cagliari and INFN, Cagliari, Italy*

[10]*IPN, Université, de Paris-Sud and CNRS-IN2P3, Orsay, France*

[11]*Università del Piemonte Orientale, Alessandria and INFN, Alessandria, Italy*

[12]*INR, Moscow, Russia*

[13]*CERN, Geneva, Switzerland*

(Received 20 June 2003; published 12 March 2004)

The fission of lead projectiles has been investigated at the CERN SPS by the NA50 experiment. For this study, a Cherenkov quartz detector was added to the standard NA50 setup to measure the charge of projectilelike fragments. The data collected on different targets at 40 and 158 GeV/*c* per nucleon are presented here. The contributions arising from the nuclear and the electromagnetic fission mechanism are extracted from the measured fission cross sections; the electromagnetic contribution is then compared to the Weizsäcker-Williams predictions.

DOI: 10.1103/PhysRevC.69.034904 PACS number(s): 25.75.−q, 25.70.Mn, 25.85.Ge

I. INTRODUCTION

In heavy-ion collisions at ultrarelativistic energies, fission can be due to both nuclear and electromagnetic processes. The interaction, which is dominated by the strong nuclear force when the colliding nuclei come into contact, becomes purely electromagnetic at impact parameters greater than the sum of the nuclear radii, where only the long-range Coulomb force plays a role.

Fission of 158*A* GeV/*c* lead projectiles impinging on a 12 mm thick lead target was observed in an experimental measurement by the NA50 experiment at the CERN SPS [1]. Although the yield of the observed fission events is roughly consistent with the one expected in case of Coulomb fission, it is clear that no firm conclusion on the fission mechanism can be drawn from this single data point. More light on the contributions of nuclear and electromagnetic mechanisms to the fission cross sections is expected to be shed by measurements on different target nuclei at different incident energies, since the dependence of the fission cross section as a function of the incident energy and of the target nucleus mass (or charge) is different for the two mechanisms. For this reason, new fission data have been taken, respectively, at 158 and 40 GeV/*c* per nucleon with a ^{208}Pb beam impinging on different target nuclei: C, Al, Cu, Ag, Pb.

This paper reports the results of these studies, carried out in the frame of the NA50 experiment at the CERN SPS. According to a model-dependent analysis, the contributions arising from the nuclear and electromagnetic fission mechanisms are extracted from the measured cross sections. The electromagnetic contribution is then compared with the Weizsäcker-Williams model predictions [6].

*Also at IST, Universidade Técnica de Lisboa, Lisbon, Portugal.

†Also at Faculty of Physics and Nuclear Techniques, Academy of Mining and Metallurgy, Cracow, Poland.

‡On leave from YerPhI, Yerevan, Armenia.

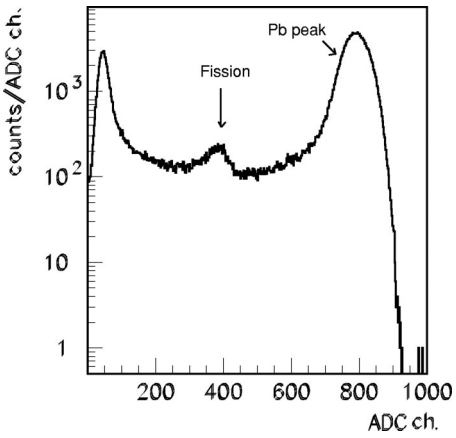

FIG. 1. Light output (ADC channels) measured by the fragment detector in Pb-Pb collisions at 158*A* GeV/*c* (ZDC trigger) [1].

II. EXPERIMENTAL APPARATUS

The main goal of the NA50 experiment is the study of the J/ψ suppression in Pb-Pb collisions as a signature of quark gluon plasma formation [2]. For a detailed description of the standard NA50 setup see Ref. [3]. For the fission measurements, a Cherenkov fragment detector (FD) has been placed on the beam trajectory downstream from the target, just in front of the zero-degree calorimeter (ZDC) which measures the energy of the spectator fragments of the projectile [4]. Since the yield of Cherenkov light is proportional to the squared charge of the particle, the quantity measured by the FD is the sum of the squared charges of the fragments emitted in the decay of the projectile (ΣZ_i^2). More details on the fragment detector and on the experimental layout can be found in Ref. [1]. In the same paper, the analog-to-digital converter (ADC) distribution of the fragment detector shown in Fig. 1 is also reported.

In the figure there is a peak, centered at channel 800, corresponding to the incoming lead ions, which have not interacted in the target and a second peak centered at channel 400, which has been interpreted as a signal of symmetric or quasisymmetric binary Pb fission [1]. The information provided by the ZDC has allowed us to confirm that fission occurs in extremely peripheral collisions.

III. RUN CONDITIONS AND DATA ANALYSIS

Although the apparatus used for the measurements reported in this paper was basically the same as the one leading to the results of Ref. [1], the experimental conditions were quite different. In fact, while previous data had been taken in parallel to the standard NA50 runs, (i.e., in conditions optimized for charmonium detection), the present data were collected during two short, dedicated runs with lower beam intensities (few times 10^5 Pb ions per burst) and thinner targets (1–4 mm). These last experimental conditions avoid pileup corrections and minimize contribution to fission of projectiles different from ^{208}Pb, as lighter Pb isotopes and heavy nuclei produced mainly by electromagnetic (e.m.) dissociation of the beam in the target (see the Appendix).

Moreover, a different trigger strategy was adopted to speed up the data taking. In Ref. [1], data acquisition was enabled by the so-called ZDC trigger. This trigger is generated when an energy larger than a given threshold E_{th} is deposited in the ZDC. Since even in the most central collisions a residual energy $E_{min} \sim 2-3$ TeV is emitted in the acceptance of the ZDC and since the threshold value was chosen in such a way that $E_{th} < E_{min}$, the ZDC trigger allows us to collect an *unbiased* sample of events, ranging from central to noninteracting Pb ions. In the analysis of the previous data, the fission cross section was directly deduced from the *unbiased* light output distribution of the fragment detector, shown in Fig. 1, by computing the ratio between the number of events in the fission peak and the total number of events in the histogram (see Ref. [1] for more details). It is clear that this approach, based on the ZDC trigger only, imposes severe limitations on the statistics achievable for fission events. In fact, even at low beam intensities, the acquisition system is saturated by the high rate of noninteracting Pb projectiles which, as can be seen in Fig. 1, dominates the sample of events collected with the ZDC trigger, while only a small fraction corresponds to fission events.

To increase the fission sample, in the latest data taking, besides the ZDC trigger, a second one, called the ZDC-VETOED trigger, was also used. This trigger is generated by requiring, in coincidence with a ZDC trigger, a signal from the fragment detector with amplitude smaller than the one of noninteracting beam. In this way, the Pb ions which did not interact in the target are rejected, as can be seen in Fig. 2 where the light output distributions recorded with this trigger on different targets are shown. It is important to underline that the fragment detector, rather than the ZDC, has been used to perform such a rejection. This is due to its better resolution for Pb ions (4% for the fragment detector, 7% for the ZDC) and to the fact that, for extremely peripheral collisions, the quantity ΣZ_i^2, measured by the fragment detector, is more sensitive to the impact parameter than the zero-degree energy measured by the ZDC (see Ref. [1]).

The number of fission events n_f is obtained by integrating the fission peak in the ADC spectrum obtained with the ZDC-VETOED trigger where the statistics for fission events is higher.

Therefore the fission cross section is calculated as

$$\sigma_f = \frac{n_f}{K N_p n_t}, \tag{1}$$

where N_p is the number of incident lead ions, n_t is the number of target nuclei per cm^2, and K is a correction factor for fission fragment reinteraction and projectile absorption prior to the fission (see the Appendix).

For the ZDC-VETOED runs, N_p has been evaluated by comparing the ADC spectra taken with ZDC and ZDC-VETOED triggers. We have integrated the first spectrum up to an ADC channel below the noninteracting lead ions peak (e.g., ADC channel 650) getting $n(zdc)$ and the second one (which does not contain the Pb peak) up to the same ADC channel getting $n(zdc\ vetoed)$. From the ratio of the obtained values we have deduced N_p for ZDC-VETOED runs:

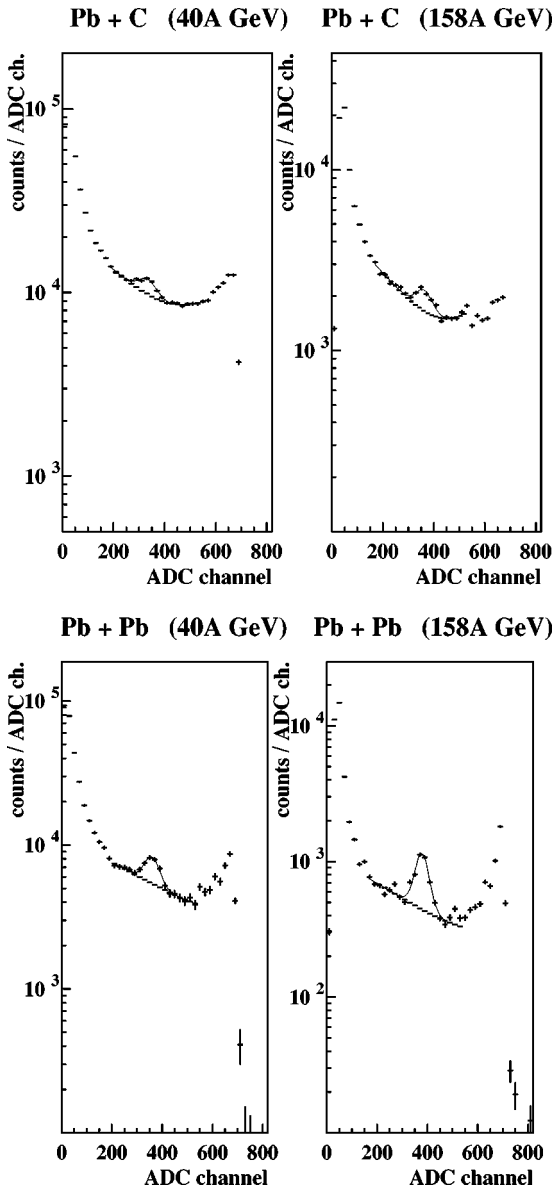

FIG. 2. Light output (ADC) measured by the fragment detector for C (top) and Pb target (bottom) at 40*A* GeV/*c* (left) and 158*A* GeV/*c* (right). The solid line is the fit to the fission peak, the dotted line is the fit to the continuum lying under the fission peak (ZDC-VETOED trigger).

$$N_p(zdc\ vetoed) = N_p(zdc)\frac{n(zdc\ vetoed)}{n(zdc)}.$$

IV. EXPERIMENTAL RESULTS

The measurements have been performed using the ^{208}Pb beam delivered by the CERN SPS at two different momenta of 40 and 158 GeV/*c* per nucleon. About one million events were collected for each target, namely, C (4 mm thick), Cu (3.2 mm), Ag (3 mm), Pb (3 mm) at 40*A* GeV/*c* and C (4 mm), Al (3 mm), Cu (1 mm), Ag (1 mm), Pb (4 mm) at 158*A* GeV/*c*.

TABLE I. Experimental fission cross sections values at 40*A* GeV/*c* and 158*A* GeV/*c*.

	σ_f (mb)—40*A* GeV/*c*	σ_f (mb)—158*A* GeV/*c*
C	27.8±2.6	30.0±3.0
Al		56.0±5.0
Cu	49.1±5.0	77.0±11.0
Ag	60.1±5.3	129.0±14.0
Pb	120.5±9.5	332.0±19.0

Figure 2 shows the ADC spectra of the fragment detector in Pb-C and Pb-Pb interactions at 40 and 158 GeV/*c* per nucleon, after the subtraction of the pedestal and of the *empty target* contribution, which in the fission region of the spectrum ranges from 60% to 85%. This important empty target contribution is essentially due to the fact that the lead ions travel along 160 cm of air between the target and the fragment detector.

The spectra shown in Fig. 2 have been obtained with the ZDC-VETOED trigger. The fission peak and the underlying continuum have been fitted simultaneously with a polynomial plus a variable width Gaussian function. The numbers of fission events have been extracted from the fit to the ADC spectrum, by subtracting from the fission peak the background contribution as provided by the polynomial function of the fit.

Experimental fission cross sections are reported in Table I and plotted in Fig. 3 as a function of the target atomic number Z_t at 40 and 158 GeV/*c* per nucleon. The reported errors are mainly due to the uncertainty in the extrapolation of the continuum under the fission peak. For lighter targets there is no major difference between data at the two energies; for heavier targets the fission cross sections at 158*A* GeV/*c* become larger and larger with Z_t than the ones at 40*A* GeV/*c*. At both energies the fission cross section increases with Z_t.

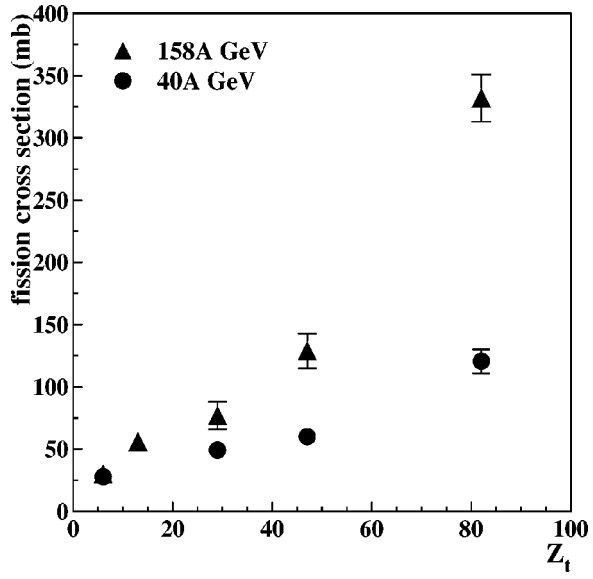

FIG. 3. Experimental fission cross sections as a function of Z_t at 40*A* GeV/*c* (full circles) and 158*A* GeV/*c* (full triangles).

The Pb-Pb fission cross section measured in this experiment at 158*A* GeV/*c* is consistent with the one (about 340 mb) reported by the emulsion experiment EMU13 [5].

V. FISSION MECHANISM

In heavy-ion collisions, fission can be induced both by electromagnetic and nuclear interactions. Therefore the total fission cross section can be expressed as the sum of the contributions arising from these two mechanisms:

$$\sigma_f = \sigma_f^C + \sigma_f^N.$$

This approximation can be justified by the short range of the nuclear force, which contributes only when the nuclei come into contact. At larger impact parameter b (greater than the sum of the radii of the two colliding nuclei) the nuclear fission mechanism vanishes and the fission cross section is assumed to be entirely due to the e.m. interaction. In reality there is a small but finite region of b (close to the sum of the nuclear radii) where both processes can occur, but the magnitude of such interference effects has been estimated with an idealized form of the nucleon-nucleon interaction, and was found to be less than 1% of the total cross section [7].

In order to disentangle the two contributions to the measured fission cross sections, the different behavior of σ_f^C and σ_f^N as a function of the target atomic number and target mass number can be considered. For this purpose, the dependence of σ_f^C and σ_f^N, respectively, on Z_t and A_t are estimated in Secs. V A and V B. In Sec. V C these dependences are used to fit the data and to extract the two contributions.

A. Coulomb fission cross section

The electromagnetic processes become dominant when the projectile and the target nuclei collide at impact parameters b larger than the sum of the nuclear radii (i.e., $b > b_{min} \approx R_p + R_t$).

According to the Weizsäcker-Williams (WW) method [6], the e.m. interaction between two nuclei can be expressed in terms of the interaction of the projectile nucleus with a virtual photon emitted by the target nucleus, which may induce the fission of the projectile.

The Coulomb fission cross section of the projectile nucleus is determined by the equivalent photon spectrum $n_t(\omega)$ of the target nucleus, multiplied by the photofission cross section $\sigma_{\gamma f}(\omega)$ of the projectile nucleus. For the computation of σ_f^C we must integrate over all photon energies ω:

$$\sigma_f^C = \int n_t(\omega)\sigma_{\gamma f}(\omega)d\omega. \quad (2)$$

The expression for the equivalent photon distribution can be derived in the frame of classical electromagnetism [8]. The WW method was extended by including higher multipolarities πl [9] in the equivalent photon spectrum. The resulting number of virtual photons, integrated over the impact parameter, is given by

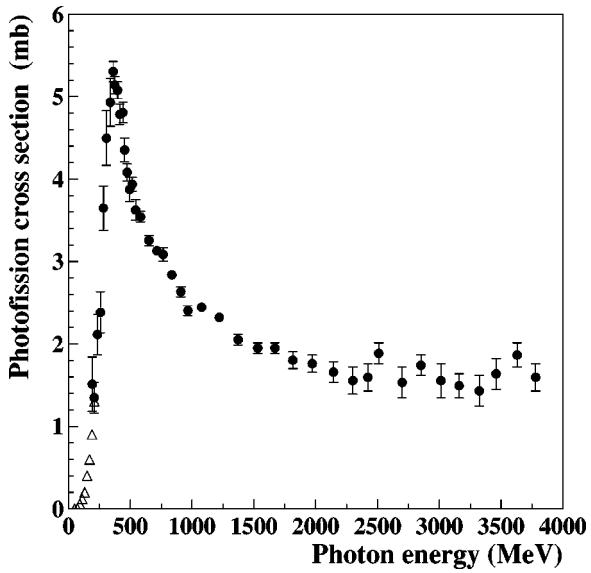

FIG. 4. Photofission cross sections for ^{nat}Pb (from Ref. [10]) as a function of the incident photon energy. For photon energy values below 0.17 GeV data from Ref. [11] are used (open triangles).

$$n_t(\omega) = \frac{2Z_t^2\alpha}{\pi\omega\beta^2}\left(\xi K_0(\xi)K_1(\xi) - \frac{\beta^2\xi^2}{2}[K_1^2(\xi) - K_0^2(\xi)]\right), \quad (3)$$

where α is the fine structure constant, K_0 and K_1 are the modified Bessel functions of order zero and one, $\xi = \omega b_{min}/\beta\gamma$ (where γ is the Lorentz factor of the target nucleus in the rest frame of the projectile nucleus), and b_{min} is the cutoff impact parameter below which nuclear processes take over and become dominant.

Benesh, Cook, and Vary [7] proposed the following parametrization for b_{min}:

$$b_{min}^{BCV} = r_0[A_p^{1/3} + A_t^{1/3} - x(A_p^{-1/3} + A_t^{-1/3})], \quad (4)$$

where A_p and A_t are the mass number of the projectile and the target nuclei, $r_0 = 1.34$ fm, and $x = 0.75$.

To compute the Coulomb fission cross section for ^{208}Pb-nucleus interactions at 158 and 40 GeV/*c* per nucleon, the photofission cross section of ^{208}Pb should be used as input of Eq. (2). Indeed, due to the lack of photofission data for ^{208}Pb over the full energy range of the virtual photons emitted at SPS energies (from the ^{208}Pb fission threshold of 28 MeV up to about 2 GeV), the following strategy has been adopted. For photon energies below 0.17 GeV the photofission cross section for ^{208}Pb was taken from Ref. [11], while at higher energies the ^{nat}Pb photofission values recently measured at the Jefferson Laboratory in the energy interval $\omega = 0.17-3.84$ GeV [10] have been used (Fig. 4).

In order to determine the behavior (i.e., the slope as a function of Z_t) of the σ_f^C values, the computed Coulomb fission cross sections have been fitted as $\sigma_f^C = \sigma_0 Z_t^\delta$. The obtained values for δ are 1.72 and 1.86, respectively, at 40 and 158 GeV/*c* per nucleon. It is worth noting that values of the δ parameter slightly smaller than two are due to the fact that

the Z_t^2 dependence of Eq. (3) is reduced by the increase of the minimum impact parameter b_{min} with the target radius [Eq. (4)].

B. Nuclear fission cross section

The nuclear contribution σ_f^N to the fission cross section can be computed according to the geometrical scaling model proposed in Ref. [12], developed to interpret uranium fission data on several targets at 120*A* MeV. As only the most peripheral collisions are expected to contribute, we can consider the region of impact parameter ranging from $b_{min}-\Delta b$ to b_{min}, which defines an annulus of width Δb whose area gives the cross section for nuclear fission

$$\sigma_f^N = 2\pi \times \Delta b\left(b_{min} - a - \frac{\Delta b}{2}\right), \tag{5}$$

where

$$a = \frac{Z_p Z_t e^2}{\mu\beta^2\gamma}$$

corrects for the Rutherford bending of the trajectory [13].

In the measurements reported here the Rutherford correction term is negligible because of the high beam energies.

In order to apply this geometrical model to the ^{208}Pb fission, the fact that the fissility of ^{208}Pb, unlike that of uranium, is smaller than one must be taken into account. Therefore Eq. (5) has been multiplied by a correction factor f, which represents the probability for ^{208}Pb to undergo fission, when a collision with impact parameter between $b_{min}-\Delta b$ and b_{min} has taken place. Moreover the second-order term in Δb can been neglected, since for uranium a Δb value of about 0.8 fm was found in Ref. [12].

The nuclear contribution to the lead fission cross section at SPS energies has been finally approximated as

$$\sigma_f^N = 2\pi f b_{min}\Delta b, \tag{6}$$

where b_{min} has been computed according to Eq. (4). This means that, in contrast to the predicted $Z_t^{1.72}$ at 40*A* GeV/*c* ($Z_t^{1.86}$ at 158*A* GeV/*c*) rise of σ_f^C, σ_f^N is expected to increase more slowly for heavy targets (as $A_t^{1/3}+A_p^{1/3}$).

C. Experimental results interpretation

In this section the experimental data are interpreted in the light of the previous considerations. Let us consider again the measured fission cross sections shown in Fig. 3. As previously stated, the energy dependence of the fission cross section is negligible for the carbon target and becomes more and more pronounced for higher values of Z_t. Such a behavior suggests that for light targets the relevant fission mechanism is the nuclear one (which is expected to exhibit a weak dependence on the incident energy), while the e.m. contribution (which has a much stronger energy dependence) becomes dominant for heavy targets. This interpretation is consistent with the fact that, as discussed in Secs. V A and V B, the e.m. contribution increases much faster than the nuclear one as a function of the mass (or charge) of the target

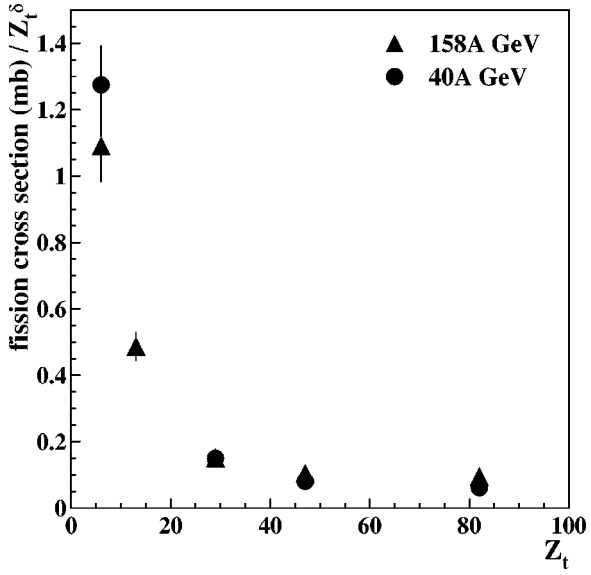

FIG. 5. Experimental fission cross sections divided by Z_t^δ as a function of Z_t at 40*A* GeV/*c* (full circles) and 158*A* GeV/*c* (full triangles).

nucleus. Moreover, this is also supported by the behavior of the fission cross section divided by Z_t^δ (where $\delta=1.72$ and $\delta=1.86$ were determined, respectively, at 40 and 158 GeV/*c* per nucleon, as described in Sec. V A), plotted versus Z_t (Fig. 5). Indeed the ratio is constant only for heavy targets and becomes larger for low values of Z_t, indicating that for light targets the e.m. mechanism alone cannot account for the measured cross section and the nuclear one plays a significant role.

In order to extract the nuclear and e.m. contributions from the experimental fission cross sections, data have been fitted as the sum of a term proportional to Z_t^δ (e.m. contribution) and a nuclear term given by Eq. (6):

$$\sigma_f = \sigma_f^C + \sigma_f^N = c_1 Z_t^\delta + 2\pi c_2 b_{min}, \tag{7}$$

where the δ exponent has been fixed as described in Secs. V A, while c_1 and c_2 are free parameters. In particular c_2 is equal to the product $\Delta b f$ [see Eq. (6)] and its value given by the fit is 0.0411 ± 0.035 fm (0.0497 ± 0.040 fm) at 40(158)GeV/*c* per nucleon. For the sake of completeness, we note that, even if only the product $\Delta b f$ can be deduced from the fit, an indication about the value of the parameter f can be obtained by dividing c_2 by $\Delta b \simeq 0.8$ fm, found for uranium and reported in Refs. [12,13]. This calculation gives $f \simeq 0.05-0.06$, a value of the same order of magnitude of the fissility, which is about $(8\pm1)\%$ for ^{nat}Pb [14].

The values of the c_1 parameters obtained from the fit are 0.0388 ± 0.0049 mb and 0.0768 ± 0.0049 mb, respectively, at 40 and 158 GeV/*c* per nucleon.

The e.m. (σ_f^C) and nuclear (σ_f^N) contributions to the fission cross sections deduced from the fit to the experimental data are displayed in Figs. 6 and 7 for incoming ^{208}Pb beams of 40 and 158 GeV/*c* per nucleon (Table II). As expected, the nuclear term increases very weakly with the target mass, while the e.m. contribution, negligible for light targets, be-

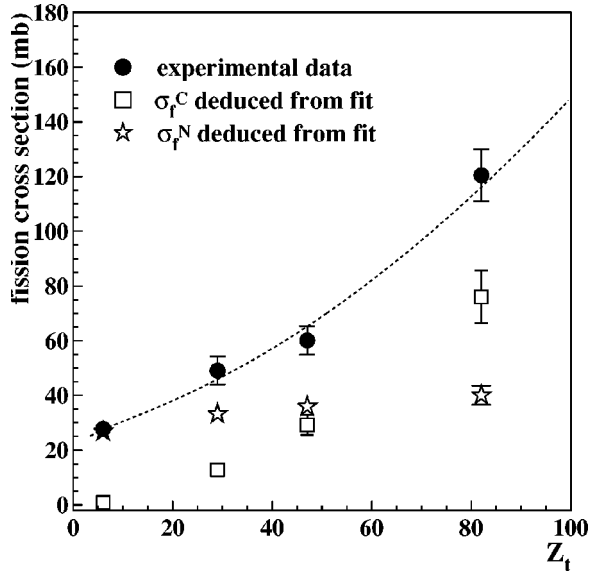

FIG. 6. Experimental fission cross sections as a function of Z_t at 40*A* GeV/*c* (full circles). The dotted line is the fit to the data according to Eq. (7). σ_f^C (open squares) and σ_f^N (open stars) deduced from the fit are also reported.

comes dominant for heavier ones. Moreover, the e.m. term quickly increases as a function of energy, as shown in Fig. 8.

In Figs. 9 and 10 the e.m. contributions to the fission cross section, deduced from the fit to the experimental σ_f results, are compared to the WW model predictions computed by means of Eq. (2) by using the $\sigma_{\gamma f}$ values from Ref. [10], as described in Sec. V A. A satisfactory description of the extracted e.m. contributions is obtained at 158*A* GeV/*c* and for light targets at 40*A* GeV/*c*. On the contrary, the WW predictions for Pb-Pb interactions at 40*A* GeV/*c* are significantly below the value of the e.m. contribution to the fission cross

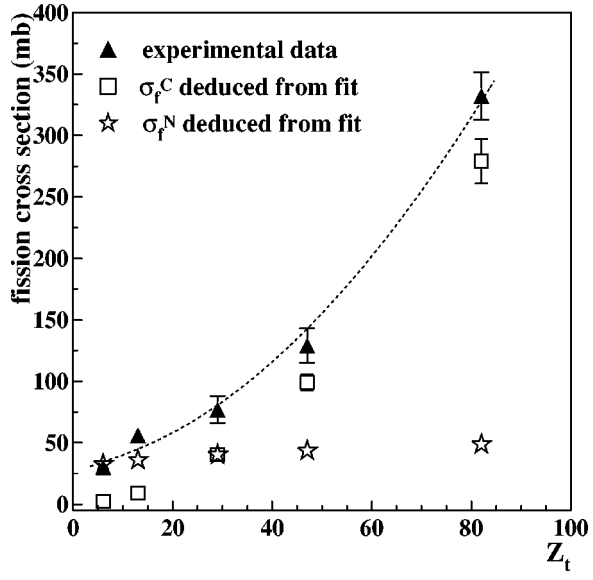

FIG. 7. Experimental fission cross sections as a function of Z_t at 158*A* GeV/*c* (full triangles). The dotted line is the fit to the data according to Eq. (7). σ_f^C (open squares) and σ_f^N (open stars) deduced from the fit are also reported.

TABLE II. Nuclear and Coulomb fission cross sections values at 40*A* GeV/*c* and 158*A* GeV/*c* extracted from the fit to the data.

	σ_f^N (mb) 40*A* GeV/*c*	σ_f^N (mb) 158*A* GeV/*c*	σ_f^C (mb) 40*A* GeV/*c*	σ_f^C (mb) 158*A* GeV/*c*
C	26.8±2.3	32.5±2.6	0.8±0.1	2.1±0.1
Al		35.8±2.9		9.1±0.6
Cu	33.2±2.8	40.2±3.2	12.7±1.6	40.4±2.6
Ag	35.9±3.1	43.5±3.5	29.2±3.7	99.0±6.4
Pb	40.0±3.4	48.5±3.9	76.0±9.6	278.9±18.0

section. Since the latter has been deduced assuming the nuclear term scaling of Ref. [12], the observed discrepancy suggests a faster increase of the nuclear contribution (as a function of the target mass) than the one assumed in the model [Eqs. (6) and (4)]. We note that this effect plays a minor role at 158*A* GeV/*c* since at this energy the fission cross section is dominated by the e.m. contribution (see Fig. 7).

Therefore an alternative method based on the factorization model [18] has been applied in order to deduce the target dependence of the nuclear fission cross section.

First of all we assume that the continuum events under the fission peak (see Fig. 2) are mainly originated in nuclear collisions. This argument is supported by the fact that the underlying continuum events occur in peripheral interactions where the mean value of the ZDC energy is 500–800 GeV lower than the Pb incident energy. This indicates the presence of at least 3–5 participant nucleons (see Fig. 5 of Ref. [1]).

According to the factorization model we therefore assume that the target dependences of the cross sections for the nuclear fission and for the continuum under the fission peak

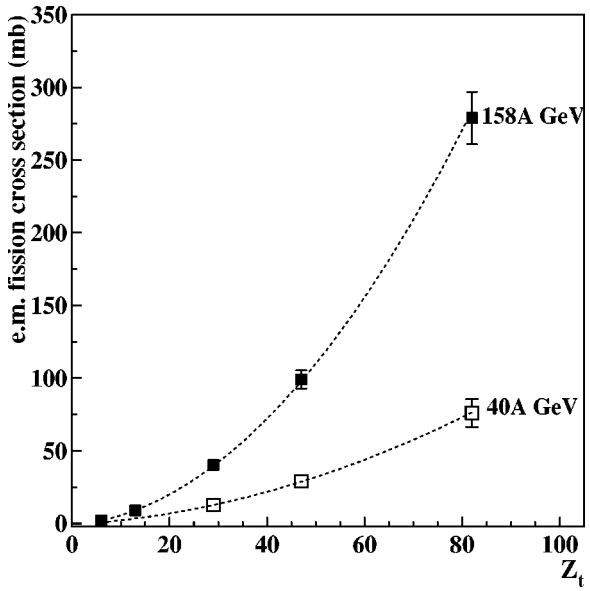

FIG. 8. e.m. fission cross sections deduced from the fit to the experimental data as a function of Z_t at 40*A* GeV/*c* (open squares) and 158*A* GeV/*c* (full squares).

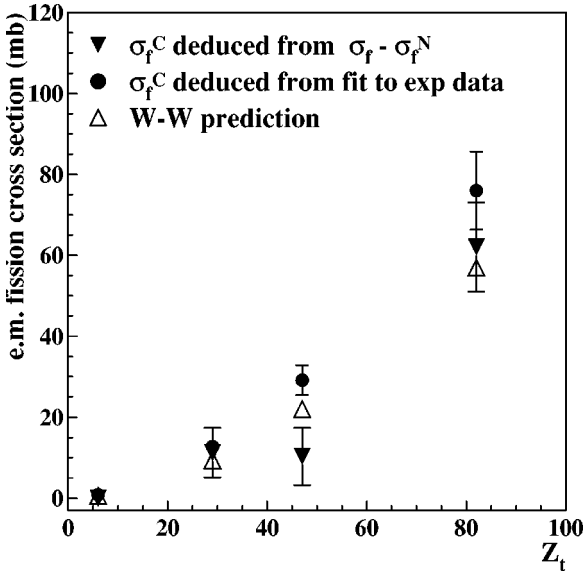

FIG. 9. e.m. contributions to the fission cross section as a function of Z_t at 40*A* GeV/*c*: extracted from the fit to the data (full circles), extracted from data with the second method (full triangles), WW predictions (open triangles).

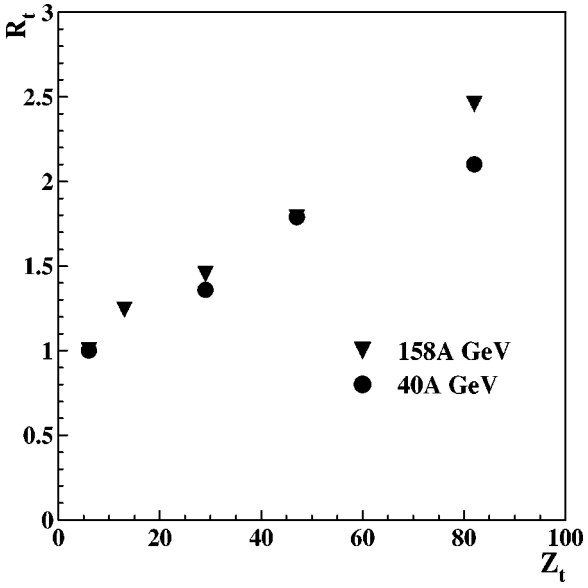

FIG. 11. Cross section ratios R_t for different targets as a function of the Z_t at 40*A* GeV/*c* (full circles) and 158*A* GeV/*c* (full triangles). The error bars are not visible since they are smaller than the symbols.

are the same. The cross sections for the latter process have been extracted from the measured light output spectra and the ratios of the cross section on the different targets to the one on carbon are shown in Fig. 11. It has been verified that, for all the targets, the integrated events correspond to the same fraction of the inelastic cross section (about 9%).

The values of the R_t ratios measured at 40 and 158*A* GeV/*c* are very close. This weak energy dependence corroborates the idea that the continuum under the fission peak is due to nuclear interactions. Nevertheless for the Pb target, the point at 158*A* GeV/*c* is significantly higher than at 40*A* GeV/*c*, suggesting that at the highest bombarding energy and for the heaviest target the e.m. contribution to the underlying continuum becomes non-negligible. Therefore, for the analysis in the frame of the factorization model, only the R_t ratios obtained at 40*A* GeV/*c* were used, excepted for the Al target where, due to the lack of data at 40*A* GeV/*c*, the R_t value measured at 158*A* GeV/*c* was used.

Hence the values of the nuclear contribution to the fission cross section σ_f^N for the different targets have been deduced by multiplying the ratios R_t by the fission cross section for the carbon target at 40*A* GeV/*c*, which has been assumed to be only nuclear. Finally the e.m. contributions to the fission cross section have been extracted by subtracting from the measured fission cross sections the nuclear contributions $(\sigma_f - \sigma_f^N)$ (Table III).

In Figs. 9 and 10 the e.m. contributions to the fission cross section, obtained with this alternative method, are compared to the ones deduced from the fit. The results obtained with the two different methods are in good agreement at 158*A* GeV/*c* and for light targets at 40*A* GeV/*c*. On the contrary the e.m. contribution for Pb-Pb and Pb-Ag interactions

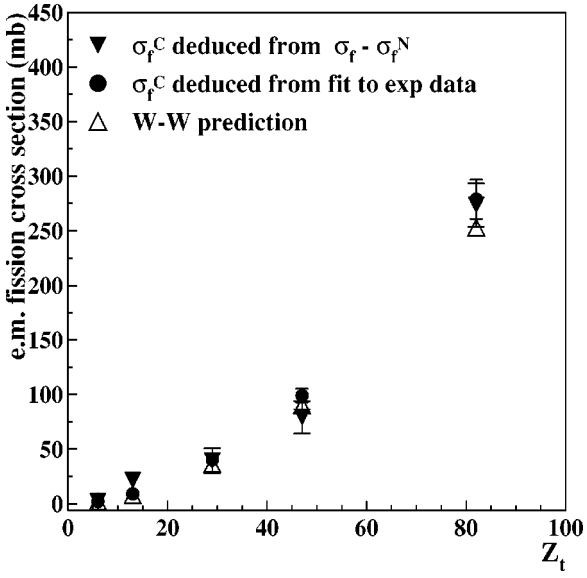

FIG. 10. e.m. contributions to the fission cross section as a function of Z_t at 158*A* GeV/*c*: extracted from the fit to the data (full circles), extracted from data with the second method (full triangles), WW predictions (open triangles).

TABLE III. Nuclear and Coulomb fission cross sections values at 40*A* GeV/*c* and 158*A* GeV/*c* extracted from data with the second method.

	σ_f^N (mb)	σ_f^C (mb) 40*A* GeV/*c*	σ_f^C (mb) 158*A* GeV/*c*
C	27.8±2.6	0.	2.2±4.0
Al	34.5±3.3		21.4±6.0
Cu	37.8±3.6	11.3±6.1	39.2±11.6
Ag	49.7±4.7	10.4±7.1	79.3±14.8
Pb	58.4±5.6	62.1±11.0	273.6±19.8

at 40*A* GeV/*c* extracted with the latter method is significantly lower than the one deduced from the fit. In particular for the Pb-Pb case, the result obtained with the factorization model is closer to the WW prediction, suggesting a nuclear target dependence stronger than the one predicted by the geometrical scaling model [12]. However, it should be noted that both the methods are enable to provide results in agreement with the WW calculations for the Ag target.

VI. CONCLUSION

Fission cross sections of lead projectiles in Pb-nucleus interactions have been measured at the CERN SPS by the NA50 experiment. In order to disentangle the electromagnetic and the nuclear contributions, measurements have been performed at two different energies (40 and 158 GeV/*c* per nucleon) and on different targets.

For this purpose a Cherenkov detector has been placed downstream of the target to provide information on the charge of the spectator fragments emitted in the decay of the ^{208}Pb projectile after its interaction in the target. A clear fission peak is visible in the ADC spectrum of the fragment detector. Information provided by the ZDC has allowed us to check that fission occurs in extremely peripheral collisions, compatible with e.m. fission or with fission induced by soft nuclear interactions involving very few participant nucleons.

Two procedures have been adopted to extract the e.m. and the nuclear contributions to the experimentally observed fission cross sections. In the first analysis, the fission cross sections have been fitted as the sum of a term proportional to Z^{δ} (where δ is fixed by the WW model predictions) and a geometrical nuclear term.

An alternative analysis based on the factorization model [18] has been carried out as well. The method is based on two relevant assumptions: the first is that the continuum under the fission peak is due to nuclear interactions and the second one is that the fission cross section on carbon at 40*A* GeV/*c* is entirely nuclear (i.e., the e.m. contribution is negligible). The e.m. term is estimated by subtracting the nuclear one from the total fission cross section. The results obtained with these two methods for the e.m. fission cross section are fully consistent at 158*A* GeV/*c* and for light targets at 40*A* GeV/*c*. The Pb-Pb point at 40*A* GeV/*c* extracted with the second method is lower than the one deduced from the fit. The e.m. contributions to the fission cross section, deduced with both the above methods, have been compared to calculations performed using the Weizsäcker–Williams approach. The comparison shows a better agreement with the values obtained with the second method, probably indicating a faster increase of the nuclear contribution as a function of the target mass than the one predicted in the geometrical scaling model [12].

Since experimental data of ^{208}Pb photofission were not available on the whole energy range of virtual photons radiated at SPS energies, we have used $^{\text{nat}}$Pb measurements for the WW calculation of e.m. contribution. A better evaluation of the W-W predictions could be performed when experimental data of ^{208}Pb photofission will be available.

Finally we have to remark that the measurements presented in this paper represent the first systematic study of lead projectile fission cross sections at ultrarelativistic energies.

ACKNOWLEDGMENTS

We would like to express our gratitude to V. Muccifora and N. Bianchi for their advices and for constructive and useful discussions. We are grateful to G. Alfarone, S. Brasolin, F. Daudo, and P. Mereu for their technical support during the construction of the fragment detector. This work was partially supported by Fundação para a Ciência e a Tecnologia.

APPENDIX

Two different corrections have been performed on the experimental data: they are included in the factor K of Eq. (1) which is the product of two terms K_1K_2.

The first correction accounts for fission fragment reinteraction, where the fission fragments originating in the target interact somewhere along the 1.6 m of air between the target and the quartz blade. These events do not appear, in fact, in the recorded fission peak. The second correction accounts for absorption within the target both of projectile Pb ions prior to a potential fission and of fission fragments for a fission event. These events are lost and disappear from the fission peak.

For the first correction factor K_1, the probability that both fission fragments do not interact along the 1.6 m of air has been estimated to be of the order of 97%, by considering only the nuclear interaction cross section for fission fragments in air, approximated by the expression [15]

$$\sigma^N = \pi r_0^2 (A_p^{1/3} + A_t^{1/3} - \delta)^2 \tag{A1}$$

with $r_0 = 1.35$ fm, $\delta = 1.1$, $A_p \simeq 100$ for the fission fragments, and $A_t \simeq 14.7$ for air. The contribution from e.m. dissociation cross section for Pb fragment-air interactions has been neglected.

For the second correction factor K_2, the probability that both the projectile Pb ion and the fission fragments do not interact within the target has been estimated to be of the order of 82–95 % depending on the target, using the following parametrization:

$$\frac{1}{l}\int_0^l P_1(x)P_2(x)dx, \tag{A2}$$

where l is the target thickness, $P_1(x)$ is the probability of finding a given Pb projectile at a depth x in the target, $P_2(x)$ is the probability that both fission fragments, produced at a depth x in the target, manage to come out of the target without interacting.

Calculations were made for all the targets, by considering

$$P_1(x) = e^{-x/\lambda_1} \quad \text{and} \quad P_2(x) = e^{-2(l-x)/\lambda_2},$$

where λ_1 and λ_2 are the total (nuclear + e.m.) mean free path in the target, respectively, of an incident Pb and of a fission fragment. The values of λ_i have been evaluated by using Eq. (A1) for the nuclear cross sections and by estimating the cross sections for the e.m. dissociation of a Pb ion or of a

fission fragment according to the WW method, by replacing in integral (2) the photofission cross sections with the photon absorption cross sections measured up to 100 GeV in Ref. [16].

For the computation of the e.m. term, we have considered that a nucleus breakup can be induced only by high energy photons ($\omega \geqslant 40$ MeV). In fact the giant dipole resonance excitation produces only the emission of one or more neutrons and does not modify the quartz blade signal.

Once $\sigma^C(\omega \geqslant 40 \text{ MeV})$ has been estimated for Pb-Pb, we have deduced its value for lighter targets assuming $\sigma^C \propto Z_t^2$, and for fragment-Pb interaction by assuming the following projectile scaling: $\sigma^C \propto N_p Z_p / A_p$ [17].

The systematic uncertainties for K_1 and K_2 have been estimated to be less than 2%.

Finally we point out that a fraction of the observed fission events is due to fission of projectiles different from ^{208}Pb. In fact, due to the target thickness, the ^{208}Pb beam has a certain probability, prior to a potential fission, to interact in the target and to transform into a lighter Pb isotope, mainly by e.m. dissociation. The fraction of fission events due to the fission of ^{208}Pb projectile turns out to be of the order of 86% (76%) for the lead targets at 40A GeV/c (158A GeV/c), while for the lighter targets this fraction is always higher than 95%. These numbers have been obtained assuming that the fission cross sections are the same for all the Pb isotopes.

[1] M. C. Abreu *et al.*, Phys. Rev. C **59**, 876 (1999).
[2] T. Matsui and H. Satz, Phys. Lett. B **178**, 416 (1986).
[3] M. Abreu *et al.*, Phys. Lett. B **410**, 327 (1997); **410**, 337 (1997).
[4] R. Arnaldi *et al.*, Nucl. Instrum. Methods Phys. Res. A **411**, 1 (1998).
[5] M. L. Cherry *et al.*, Acta Phys. Pol. B **29**, 2129 (1998).
[6] E. J. Williams *et al.*, Proc. R. Soc. London, Ser. A **139**, 163 (1933); C. F. von Weizsäcker, Z. Phys. **88**, 612 (1934).
[7] C. J. Benesh, B. C. Cook, and J. P. Vary, Phys. Rev. C **40**, 1198 (1989).
[8] M. Vidovic, M. Greiner, C. Best, and G. Soff, Phys. Rev. C **47**, 2308 (1993).
[9] C. A. Bertulani and G. Baur, Phys. Rep. **163**, 299 (1988).
[10] C. Cetina *et al.*, Phys. Rev. C **65**, 044622 (2002).
[11] L. G. Moretto, R. C. Gatti, S. G. Thompson, J. T. Routti, J. H. Hiesenbergh, L. M. Middleman, M. R. Yearian, and R. Hofstadter, Phys. Rev. **179**, 1176 (1969).
[12] M. L. Justice, Y. Blumenfeld, N. Colonna, D. N. Delis, G. Guarino, K. Hanold, J. C. Meng, G. F. Peaslee, G. J. Wozniak, and L. G. Moretto, Phys. Rev. C **49**, R5 (1994).
[13] M. L. Justice, Ph.D. thesis, University of California, Berkeley, 1991; Lawrence Berkeley Laboratory Report No. LBL 31704.
[14] C. Cetina *et al.*, Phys. Rev. Lett. **84**, 5740 (2000).
[15] H. R. Schmidt and J. Schukraft, J. Phys. G **19**, 1705 (1993).
[16] M. Vidovic, M. Greiner, and G. Soff, Phys. Rev. C **48**, 2011 (1993).
[17] B. L. Berman and S. C. Fulz, Rev. Mod. Phys. **47**, 713 (1975).
[18] Th. Rubehn *et al.*, Z. Phys. A **353**, 197 (1995).